Supplementary note 1 – Polarization-Encoded Photon-to-Spin Interface (PEPSI)

Alligator PDR

As illustrated in Supplementary Fig. 1(a), the polarization-dependent reflector (PDR) is an alligator photonic crystal (PhC) mirror that is optimized for maximizing the state fidelity given a fixed cavity reflectivity and cavity-waveguide coupling. The geometry is chosen carefully to balance losses. With $a = 184$ nm, width of $W = 2.07a$, and amplitude modulation of $dW = 3.97a$, the V transmission and H reflection coefficients are 98.3% and 86.3%, respectively, at $\lambda = 737$ nm. Both ends are adiabatically tapered ends over 10 periodicities to minimize scattering loss of the V polarization. The number of periodicities for the reflector section $N_{\text{reflector}} = 20$ is chosen to have the appropriate polarization extinction ratio (PER). Supplementary Table 1 provides the PDR transmission/reflection extinction ratios and scattering loss values for V and H obtained from finite-difference time-domain (FDTD) simulations (Lumerical Inc.).

Tunable H attenuator

To balance losses controllably, we propose adding a tunable H attenuator before the PDR. Supplementary Fig. 2 shows the implementations with both free-space optics and photonics components. Supplementary Fig. 2(a) illustrates using a beam displacer to separate out the H and V polarization modes and attenuating only the H component with a continuous variable optical filter. The two paths are subsequently recombined by a second beam displacer. In the Main text, we denote the transmission efficiency of H passing through the tunable attenuator as η_H. Despite the use of free-space optics, the two polarization modes are still effectively co-propagating, thereby maintaining the relative phase stability. Similarly, Supplementary Fig. 2(b) presents an analogous setup in a photonics platform, in which a polarization splitter diverts the H mode and a Mach-Zehnder interferometer controls the amount of H (η_H) that recombines with the V mode.

Hole-y PDR

In addition to the alligator geometry, we also explored a PhC mirror comprising a straight waveguide and air holes shown in Supplementary Fig. 3(a). The transfer fidelity is maximized at unity when the periodicity $a = 226$ nm, the air hole radius $r = 0.173a$, and the waveguide

width $W = 1.06a$. While this alternative design is more feasible in fabrication than the alligator PDR presented in the Main text, the hole-y PDR suffers from fabrication intolerance. Supplementary Fig. 3(b) indicates that the transfer fidelity worsens drastically as the air hole radius deviates only by a few nanometers, well within the margin of fabrication errors. For example, an increase in r by 2 nm from $r = 39$ nm to $r = 41$ nm lowers the fidelity to 97.3%.

Cavity parameters

Principal to the polarization encoding scheme is *detecting the phase difference* between the two spin-dependent cavity reflectivity coefficients (see Supplementary notes 2&3). Therefore, we maximize the cavity reflectivity by designing an over-coupled, single sided PhC cavity (as shown in Fig. 1(b)) with cavity-waveguide coupling $\frac{\kappa_{wg}}{\kappa} \approx 83.1\%$. It has a TM fundamental mode at ~737 nm with a loaded $Q \sim 3.5 \times 10^5$. Even accounting for a Debye-Waller factor of 0.787 [1], a radiative quantum efficiency of 9.2% [2], and a misaligned dipole orientation along the [111] direction, we calculate the cooperativity C can exceed 200. For the fidelity calculations, we assume $C = 100$ that has been experimentally demonstrated [3].

In-situ tuning

To correct for a detuned cavity resonance, we propose using an in-situ gas deposition technique [4,5] that has shown >5 nm spectral tuning. Flowing Xe gas would adhere to the surface of the diamond and introduce an additional dielectric layer, thereby red-shifting the cavity resonance. Subsequently, high-intensity laser excitation could controllably remove the deposited gas molecules to fine-tune to the desired wavelength. The same technique would also be applied to compensate for fabrication errors in the PDR.

Supplementary note 2 — State Transfer Fidelity Calculations

An incoming qubit is encoded on the polarization of a photon:

$$|\psi\rangle = \alpha|H\rangle + \beta|V\rangle \quad (1)$$

The spin qubit is initialized in an even superposition state $(|\downarrow\rangle + |\uparrow\rangle)/\sqrt{2}$, resulting in a joint spin-photon state:

$$|\psi\rangle = \alpha|H,\downarrow\rangle + \alpha|H,\uparrow\rangle + \beta|V,\downarrow\rangle + \beta|V,\uparrow\rangle \quad (2)$$

The photon hits an imperfect PDR with reflection (transmission) coefficients r_i (t_i) for the polarization $i \in \{H, V\}$. The transmitted output is incident on a nanophotonic cavity coupled to the spin qubit. While the $|\downarrow\rangle \leftrightarrow |\downarrow'\rangle$ transition is resonant with the cavity mode (see Fig. 1(a) in the main text), the $|\uparrow\rangle$ state is detuned and uncoupled to the cavity mode, such that the cavity reflection coefficients $r_{\text{cav}} \in \{r_{i,\text{coupled}}, r_{i,\text{uncoupled}}\}$ differ depending on the spin state. A self-consistent calculation basing on Supplementary Figure S4 shows that the output state is

$$|\psi_{\text{out}}\rangle = \left(r_i + \frac{r_{\text{cav}} t_i^2}{1 - r_{\text{cav}} r_i}\right) |\psi_{\text{in}}\rangle \tag{3}$$

Considering the different input states $|\psi_{in}\rangle \in \{|H,\downarrow\rangle, |H,\uparrow\rangle, |V\downarrow\rangle, |V\uparrow\rangle\}$, we denote their effective field reflectivities as:

$$|\psi_{\text{in}}\rangle = |H,\downarrow\rangle: \quad r_{H,\text{on}} = r_H + \frac{r_{H,\text{coupled}} t_H^2}{1 - r_{H,\text{coupled}} r_H} \tag{4}$$

$$|\psi_{\text{in}}\rangle = |H,\uparrow\rangle: \quad r_{H,\text{off}} = r_H + \frac{r_{H,\text{uncoupled}} t_H^2}{1 - r_{H,\text{uncoupled}} r_H} \tag{5}$$

$$|\psi_{\text{in}}\rangle = |V,\downarrow\rangle: \quad r_{V,\text{on}} = r_V + \frac{r_{V,\text{coupled}} t_V^2}{1 - r_{V,\text{coupled}} r_V} \tag{6}$$

$$|\psi_{\text{in}}\rangle = |V,\uparrow\rangle: \quad r_{V,\text{off}} = r_V + \frac{r_{V,\text{uncoupled}} t_V^2}{1 - r_{V,\text{uncoupled}} r_V} \tag{7}$$

Ideal Case: $\{t_H, r_V\} = 0, \{r_H, r_{V,\text{uncoupled}}\} = -1, t_V = 1, \{r_{H,\text{coupled}}, r_{H,\text{uncoupled}} = 0\}, r_{\text{coup}-V} = 1$

In the ideal case, the PDR is perfect and the atom coupling to the cavity is perfect with cooperativity $C \gg 1$ such that the reflection coefficient from the cavity coupled to $|\downarrow\rangle$ is +1, while all other reflections impart the usual -1 phase. This results in the state:

$$|\psi\rangle = -\alpha|H,\downarrow\rangle + \beta|V,\downarrow\rangle - \alpha|H,\uparrow\rangle - \beta|V,\uparrow\rangle \tag{8}$$

The photon is measured in the $\{D, A\}$ basis by passing it through a half waveplate (HWP) that transforms $H \to H + V, V \to V - H$ (rotation angle at $\theta = \frac{\pi}{4}$):

$$\begin{aligned} |\psi\rangle = & -\alpha|H,\downarrow\rangle - \alpha|V,\downarrow\rangle - \beta|H,\downarrow\rangle + \beta|V,\downarrow\rangle - \alpha|H,\uparrow\rangle - \alpha|V,\uparrow\rangle + \beta|H,\uparrow\rangle - \beta|V,\uparrow\rangle \\ = & |H\rangle \otimes \left((-\alpha - \beta)|\downarrow\rangle + (-\alpha + \beta)|\uparrow\rangle\right) + |V\rangle \otimes \left((-\alpha + \beta)|\downarrow\rangle - (\alpha + \beta)|\uparrow\rangle\right) \end{aligned} \tag{9}$$

After a polarizing beam splitter (PBS), detection of an $|H\rangle$ or $|V\rangle$ photon heralds mapping of the input photonic state onto the spin with a rotation that can be corrected by applying a Hadamard gate on the spin, followed by a conditional π rotation if it is detected in the H port.

General Case: General $\{r_H, t_V, r_V, t_H, r_{\text{coup}}, r_{\text{cavity}}\}$

In the general case, the entangled spin-photon state after the HWP becomes:

$$\begin{aligned}|\psi_f\rangle = |H\rangle \otimes \left[\left(\alpha r_{H,\text{on}} - \beta r_{V,\text{on}}\right)|\downarrow\rangle + \left(\alpha r_{H,\text{off}} - \beta r_{V,\text{off}}\right)|\uparrow\rangle\right] \\ + |V\rangle \otimes \left[\left(\alpha r_{H,\text{on}} + \beta r_{V,\text{on}}\right)|\downarrow\rangle + \left(\alpha r_{H,\text{off}} + \beta r_{V,\text{off}}\right)|\uparrow\rangle\right]\end{aligned} \quad (10)$$

After the PBS, projection onto the H or V basis yields the final spin state $|\psi_s(i)\rangle$, which depends on an input state $|\phi_i\rangle$. We can calculate the average state fidelity by considering the four basis states $|\phi_i\rangle$ corresponding to the *x*,*y* axes of the Bloch sphere as our input:

$$\mathcal{F} = \frac{1}{4}\Sigma_i \mathcal{F}_i = \frac{1}{4}\Sigma_i |\langle\phi_i|\psi_s(i)\rangle|^2 \quad (11)$$

Relative phases:

To account for the accumulated phase stemming from different propagation paths, the cavity reflectivities are tagged with additional phase factors $r_{\text{cav}} \rightarrow r_{\text{cav}} e^{ikL}$, in which k is the wavevector and L is the distance between the PDR and the cavity. For each polarization mode, the PDR's finite transmission and reflection extinction ratios result in two components having different phases. For example, there exists a relative phase between the transmitted V and the reflected V light. We emphasize here the PDR is designed to have minimal V transmissivity and H reflectivity. Therefore, infidelity introduced by the aforementioned phase difference is minimal. However, there does exist a non-negligible relative phase $e^{i\Delta\phi}$ *between the H and the V modes*. Due to the phase stability that is inherent in the PEPSI, we propose trimming the phase via chalcogenides [6], gas deposition [4,5], ion-implantation [7] (for the PIC approach only), or an electro-optical modulator to eliminate $e^{i\Delta\phi}$.

Supplementary note 3 – State-dependent reflectivity

The input-output formalism dictates [8,9]

$$\hat{a}_{\text{wg,out}} = \hat{a}_{\text{wg,in}} + \sqrt{\kappa_{\text{wg}}}\,\hat{a} \quad (12)$$

where $\hat{a}_{\text{wg,in}}, \hat{a}_{\text{wg,out}}$ are the input and output field annihilation operators, and $\hat{a}$ is the annihilation operator of the cavity mode. κ_{wg} is the coupling rate between the waveguide and the single-sided cavity.

The Heisenberg-Langevin equations of motion for an atom-coupled cavity QED system are:

$$\frac{d\hat{a}}{dt} = -\left[\mathrm{i}(\omega_c - \omega) + \frac{\kappa}{2}\right]\hat{a} - \mathrm{i}g\sigma_- - \sqrt{\kappa_{\mathrm{wg}}}\hat{a}_{\mathrm{wg,in}} \tag{13}$$

$$\frac{d\sigma_-}{dt} = -\left[\mathrm{i}(\omega_a - \omega) + \frac{\gamma}{2}\right]\sigma_- + \mathrm{i}g\sigma_z\hat{a} \tag{14}$$

where ω_c, ω_a are the cavity resonance and atomic transition frequencies. κ, γ and g are the cavity total decay, atom relaxation, and atom-cavity coupling rates.

Assuming the incoming field is slowly-varying, the vanishing time derivatives give rise to the following time-averaged values:

$$\langle\sigma_-\rangle = \frac{\mathrm{i}}{g}\left(\alpha\langle\hat{a}\rangle + \sqrt{\kappa_{\mathrm{wg}}}\langle\hat{a}_{\mathrm{wg,in}}\rangle\right) \tag{15}$$

$$\langle\hat{a}\rangle = \frac{\mathrm{i}\beta}{g}\langle\sigma_-\rangle \tag{16}$$

Which give us the closed forms

$$\langle\hat{a}\rangle = \frac{-\sqrt{\kappa_{\mathrm{wg}}}}{\alpha}\frac{\langle\hat{a}_{\mathrm{wg,in}}\rangle}{1+\frac{g^2}{\alpha\beta}} \tag{17}$$

$$\langle\sigma_-\rangle = \frac{ig\sqrt{\kappa_{\mathrm{wg}}}}{\alpha\beta}\frac{\langle\hat{a}_{\mathrm{wg,in}}\rangle}{1+\frac{g^2}{\alpha\beta}} \tag{18}$$

where $\alpha = \mathrm{i}(\omega_c - \omega) + \frac{\kappa}{2}, \beta = \mathrm{i}(\omega_a - \omega) + \frac{\gamma}{2}$, and $\langle\sigma_z\hat{a}\rangle \approx -\langle\hat{a}\rangle$ assuming weak excitation of the excited state population $\propto |\langle\sigma_-\rangle|^2$. In the limit of large cooperativity, the approximation holds as long as the incident rate of photons is much less than the lifetime $\langle\hat{a}_{\mathrm{wg,in}}{}^{\dagger}\hat{a}_{\mathrm{wg,in}}\rangle \ll g^2/\kappa_{\mathrm{wg}}$ [10,11]. For the considered cavity system, we lower the repetition rate by a factor of 100 to satisfy the condition (see Supplementary note 4).

Inserting the above result into the input-output equation yields

$$r_{\mathrm{cav}}(\omega) = \frac{\langle\hat{a}_{\mathrm{wg,out}}\rangle}{\langle\hat{a}_{\mathrm{wg,in}}\rangle} = 1 - \frac{\kappa_{\mathrm{wg}}}{\alpha}\frac{1}{1+\frac{g^2}{\alpha\beta}} \tag{19}$$

On resonance where $\omega = \omega_c = \omega_a$, the large cooperativity limit leads to a state-dependent reflectivity coefficient

$$r_{\mathrm{cav}} = \frac{C-1}{C+1} \tag{20}$$

where $C = \frac{4g^2}{\kappa\gamma}$ is the cooperativity [10]. In the uncoupled case, we take $g = 0$ and a bare reflection off the cavity gives the photon a -1 phase. On the other hand, the coupled transition

gives a +1 phase. The relative phase conditioned on the atomic state forms the basis behind the state transfer protocol detailed in Ref [12].

Tailored to the given PEPSI geometry (Supplementary note 1), we have V cavity reflection coefficients $\left|r_{V,\text{uncoupled}}\right|^2 = 43.7\%$ and $\left|r_{V,\text{coupled}}\right|^2 = 96.7\%$. The H polarization mode simply reflects off the cavity's Bragg mirrors with efficiency 95.8%.

Supplementary note 4 – State transfer rate calculations

Fidelity upper and lower bounds

Supplementary Fig. 5 shows representative curves for four selected link losses: 5,10,15,20 dB. For low loss at 5 dB, the fidelity rapidly drops off with increasing N_{attempt} since the photon would likely be lost from scattering off the device after reaching the spin. In contrast, the fidelity decreases relatively slowly at a higher link loss, e.g. 20 dB. Regardless of link losses, there exists a lower bound for the state fidelity determined purely by PDR scattering loss. If we take the limit of large N (Eq. 3 in the main text), the equation simplifies to

$$\lim_{N\to\infty} P_{\text{error}} = 1 - \frac{p_{\text{det}}}{1-p_{\text{lost}}} \tag{21}$$

The resulted lower bound for fidelity is then

$$\mathcal{F}_{\text{lower}} = \langle\rho_0\rangle - (\langle\rho_0\rangle - \tfrac{1}{2})\frac{p_{\text{det}}}{1-p_{\text{lost}}} \tag{20}$$

where $\langle\psi_{\text{ideal}}|\rho_0|\psi_{\text{ideal}}\rangle$ is $\mathcal{F}$'s upper bound is set by the single-attempt fidelity, which is $\mathcal{F}_{\text{upper}} = 99.978\%$. On the other hand, our particular device gives a lower bound $\mathcal{F}_{\text{lower}} = 90.874\%$, which stems from defining a mean fidelity conditioned on detecting a click. After a large number of attempts, at least one photon is guaranteed to arrive at PEPSI. It is either detected or lost determined by the device's efficiency. Therefore, in the $N \to \infty$ limit, $\mathcal{F}$ is purely subjected to $\frac{p_{\text{det}}}{1-p_{\text{lost}}}$.

Pulse times

τ_{pulse} is an effective pulse time that includes the fractional number of dynamical decoupling π pulses. Each π-pulse follows immediately after a series of pulses within T_2^*: $\tau_{\text{pulse}} =$

$\left(1+\frac{t_\pi}{T_2^*}\right)T_1 \times 100$, where $t_\pi = 32$ ns [1], $T_1 = 1.72$ ns is the optical lifetime [3] and $T_2^* = 0.2$ ms is the spin coherence time [11]. Note that the repetition rate is lowered by a factor of 100 to satisfy the weak excitation approximation made in Supplementary note 3.

H attenuator

We assume a transmission efficiency of 89.3% for each of the beam displacers (see Supplementary note 1) for both polarization modes. Additionally, given the specific PDR design, we set $\eta_H = 66\%$ to balance losses and maximize the transfer fidelity.

Detection system

$\eta_{det} = 93.6\%$ is the product of efficiencies of the polarizing beam splitter (PBS), the HWP, and the photon detector: 95%, 99.5%, and 99%, respectively. The numbers for the PBS and the HWP are based on commercially available components. We take the number reported in Ref. [3] for a superconducting nanowire single photon detector (SNSPD) optimized for 737 nm.

Integration platform

We calculate the state transfer rate for our proposed integration platform using the method detailed in the main text. Supplementary Fig. 6 indicates that repetition rate can be greatly increased by having multiple memories coupled to the input, thus improving the transfer rate by a factor of N_{cav} (number of cavity-coupled memories).

Supplementary note 5 – Single-attempt infidelity

FDTD simulation indicates that only $\sim 10^{-5}$ of the input H power would reach the spin qubit. In the unlikelihood that the SiV is excited, the dipole emission (with a radiative quantum efficiency of ~9.2% [2]) would result in an inefficient emission into both the H (66.6%) and V (33.4%) polarizations due to the SiV orienting along [111] and the diamond surface aligned along [100] (54.7° deviation). Much of the H light would again scatter into free space by the photonic crystal air holes, and the remaining V emission is reloaded into the waveguide with non-unity efficiency $\frac{\kappa_{\mathrm{wg}}}{\kappa} \approx 0.83$. Accounting for all the aforementioned processes, we consider the infidelity introduced by atom absorption and emission to be negligible in our single-attempt average state

fidelity calculation. For the integrated platform, on-chip polarizers can be employed to completely suppress any undesired H transmission.

FDTD simulations also indicate that there is essentially no polarization crosstalk ($< 10^{-15}$) introduced by the nanostructure. Practically, any $V \rightarrow H$ or $H \rightarrow V$ conversion would derive from fabrication errors that introduce asymmetry in the device, a factor which we do not account for in the calculations.

Supplementary note 6 – Polarization walk-off in the PIC platform

For a PIC size ~5 mm, the V light that passes through the tunable PDR would experience a small amount of polarization rotation $\propto 5$ mm/52 cm$\approx 1\%$, where the wavepacket's spatial stretch of 52 cm corresponds to the SiV's lifetime of 1.7 ns [14]. The relative phase resulted from this polarization rotation can be compensated by detecting at a basis deviated from the diagonal basis.

Supplementary note 7 – Adiabatic tapering between AlN and diamond waveguides

We simulate the transfer efficiency between an AlN waveguide and a diamond waveguide by sweeping the length of the linearly tapered region overlapped by both materials. Supplementary Fig. 7 shows that unity efficiency is possible with sufficiently adiabatic tapering.

Transmission ER (dB per period)	Reflection ER (dB per period)	V scattering loss	H scattering loss
0.886	0.947	0.5872%	12.07%

Supplementary Table 1: Specifications of alligator PDR obtained from FDTD simulations: transmission and reflection extinction ratios (ER), scattering losses for both V and H polarizations.

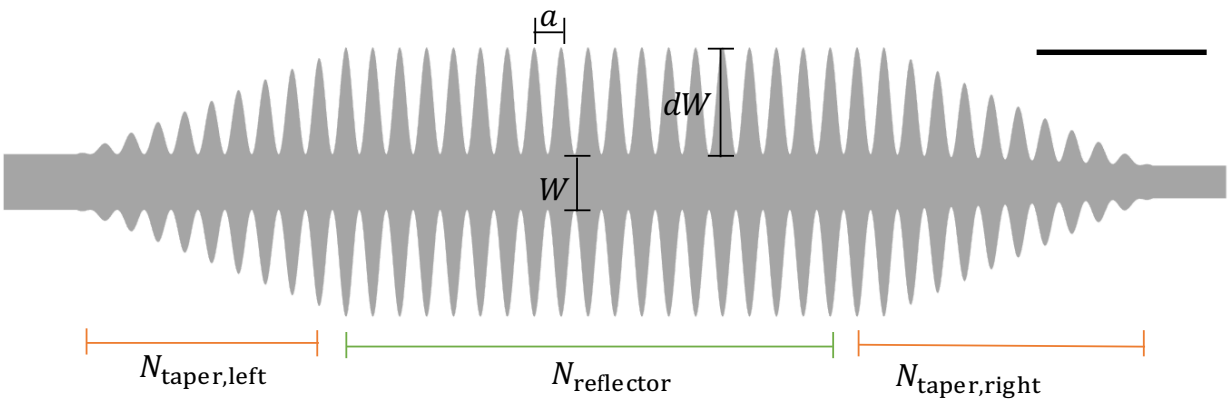

Supplementary Figure 1: Geometry of the PDR: $a = 184$ nm, width of $W = 2.07a$, and amplitude modulation of $dW = 3.97a$. The device thickness is $H = 348$ nm. The number of periodicities for the tapering and the reflector sections are: $N_{\text{taper,left}} = 10, N_{\text{reflector}} = 20, N_{\text{taper,right}} = 10$. Scale bar is 1 um.

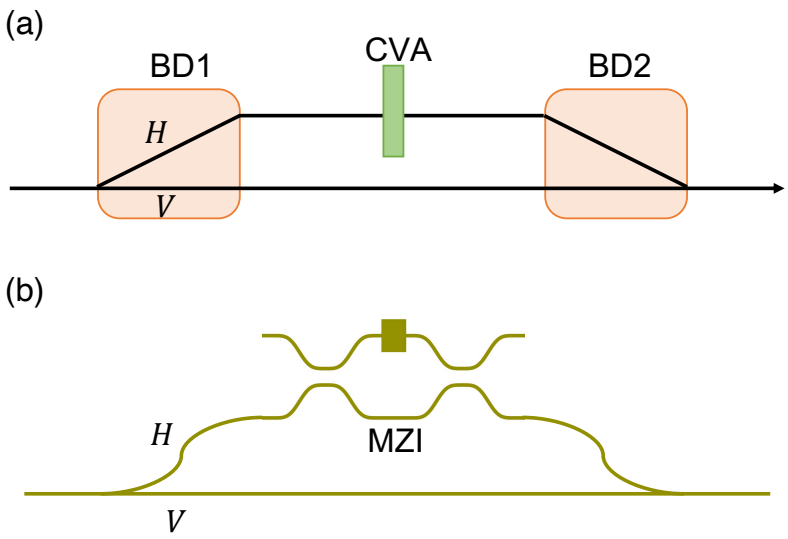

Supplementary Figure 2: Implementations of the tunable H attenuator with (a) free-space optics and (b) photonics components. (a) A beam displacer (BD1) first separates out the two polarization modes, and a subsequent continuous variable attenuator (CVA) reduces the amount of H light passing through to optimally balance losses. A second beam displacer (BD2) then recombines the two paths. (b) Analogously, in a photonics platform, a polarization splitter diverts the H polarization mode to a Mach-Zehnder interferometer (MZI), which controllably attenuates the H transmission efficiency.

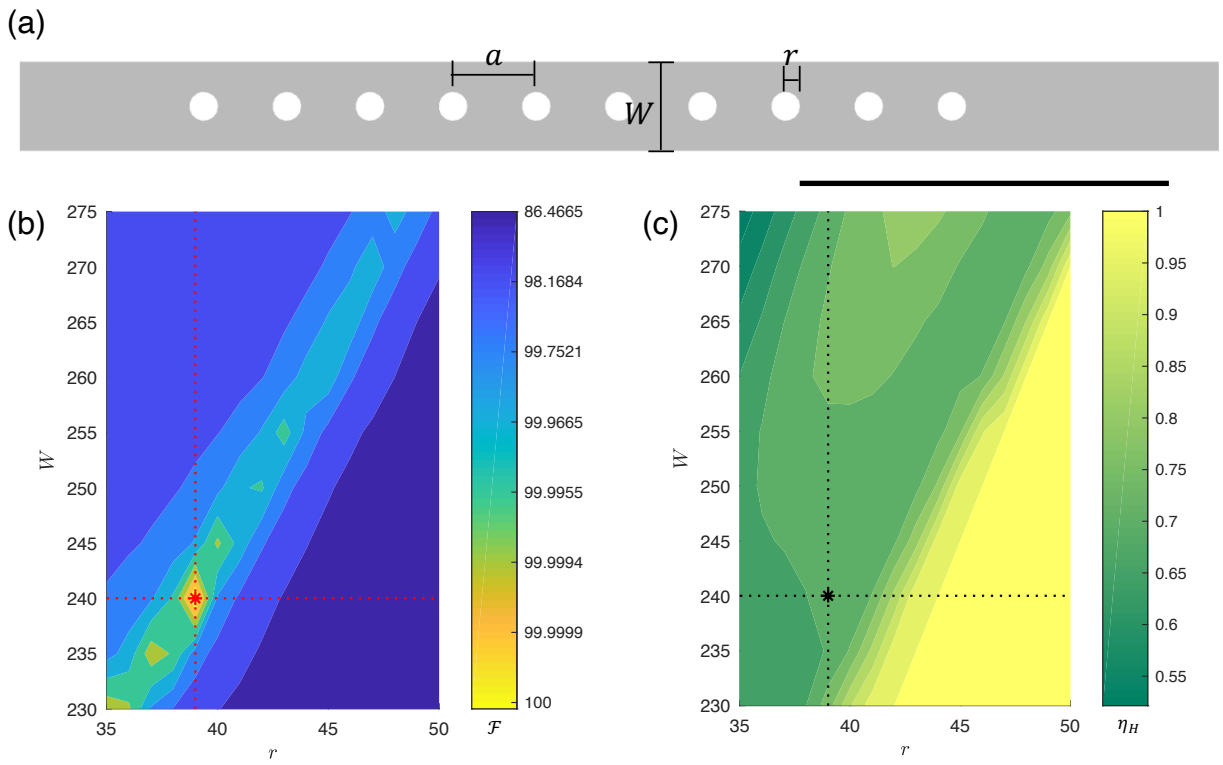

Supplementary Figure 3: (a) A PDR consisting of a straight waveguide with air holes. The geometry is defined by the periodicity $a = 226$ nm, the air hole radius $r = 0.173a$, and the waveguide width $W = 1.06a$. Scale bar is 1 um. (b) The state transfer fidelity as a function of r and W. The fidelity is maximized when $r = 39$ nm and $W = 240$ nm. (c) The corresponding H attenuation factors to optimize fidelity. At the optimal point, $\eta_H = 0.71$.

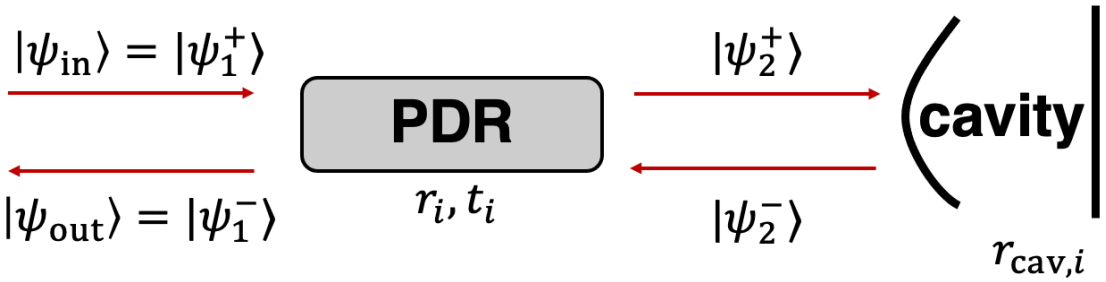

Supplementary Figure 4: Setup schematic for performing self-consistent calculations to compute the field reflectivity $r_{i,\text{on/off}} = \psi_{\text{out}}/\psi_{\text{in}}$.

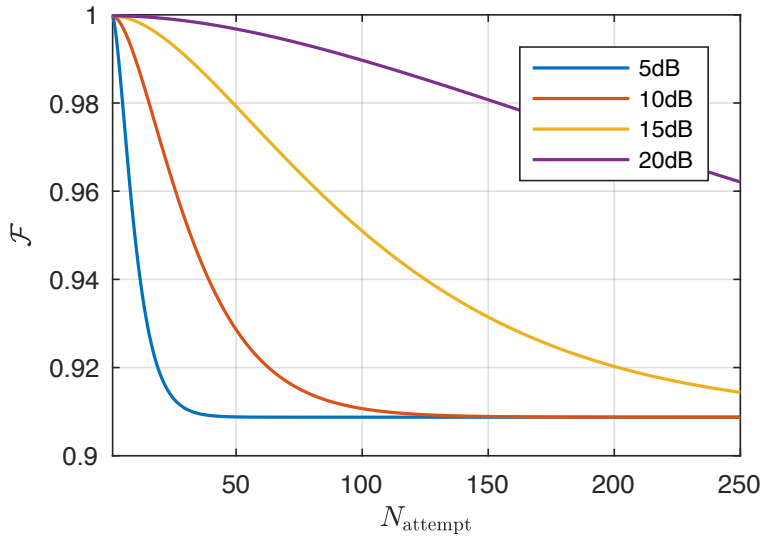

Supplementary Figure 5: Mean fidelity as a function of N_{attempt} photons at link losses 5 dB, 10 dB, 15 dB, and 20 dB. There exist a lower bound of $\mathcal{F}_{\mathrm{lower}} = 90.874\%$ and an upper bound $\mathcal{F}_{\mathrm{upper}} = 99.978\%$.

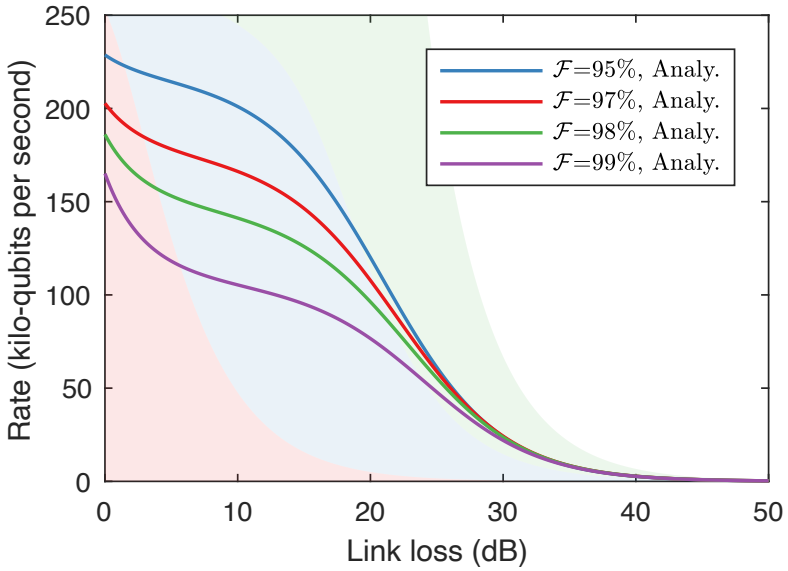

Supplementary Figure 6: Transfer rate as a function of link loss $1-\eta_{\text{link}}$ for the integration platform.

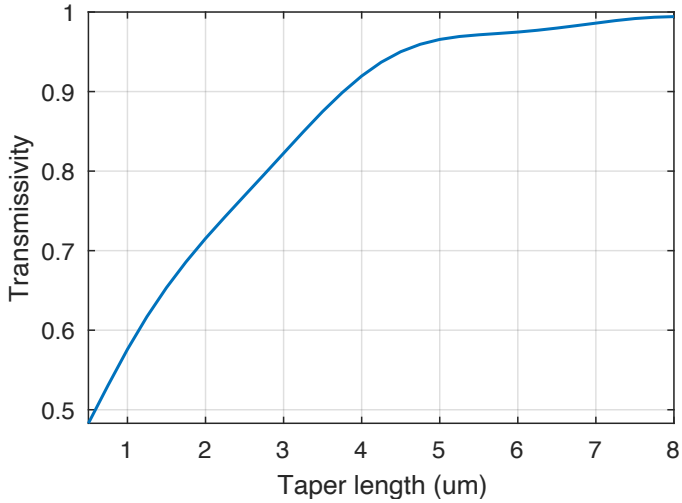

Supplementary Figure 7: The transfer efficiency between an AlN and a diamond waveguide overlapped in a linearly tapered region. The simulated transmissivity approaches unity as taper length, or adiabaticity, increases.

Supplementary References

1. E. Neu *et al.*, *New J. Phys.*, **13** 025012 (2011).
2. E. Neu, M. Agio, and C. Becher, *Opt. Express* **20**(18), 19956–19971 (2012).
3. M. K. Bhaskar *et al.*, *Nature* **580**, 60–64 (2020).
4. B. J. M. Hausmann *et al.*, *Nano Lett.* **13**, 5, 1898–1902 (2013).
5. E. R. Schmidgall *et al.*, *Nano Lett.* **18**, 2, 1175–1179 (2018).
6. A. Canciamilla *et al.*, *Opt. Express* **20** (14), 15807–15817 (2012).
7. X. Chen *et al.*, *Photon. Res.* **5** (6), 578-582 (2017).
8. A. Reiserer and G. Rempe, *Rev. Mod. Phys.* **87**, 1379 (2015).
9. E. Waks and J. Vuckovic, *Phys. Rev. Lett.* **96**, 153601 (2006).
10. E. Waks and J. Vuckovic, *Phys. Rev. A* **73**, 041803 (2006).
11. T. G. Tiecke *et al.*, *Nature* **508**, 241-244 (2014).
12. L.-M. Duan and H. J. Kimble, *Phys. Rev. Lett.* **92**, 127902 (2004).
13. L. Rogers *et al.*, *Nat. Commun.* **5**, 4739 (2014).
14. T. Schroder *et al.*, *Nat. Commun.* **8**, 15376 (2017).